

Hydrogen jump diffusion in C14-type ZrMn_2H_3 : Quasielastic neutron scattering study

A. V. Skripov,¹ T. J. Udovic,² and J. J. Rush^{2,3}

¹*Institute of Metal Physics, Urals Branch of the Academy of Sciences, Ekaterinburg 620041, Russia*

²*NIST Center for Neutron Research, National Institute of Standards and Technology, Gaithersburg, Maryland 20899-8562, USA*

³*Department of Materials Science and Engineering, University of Maryland, College Park, Maryland 20742-2115, USA*

(Received 22 May 2007; published 17 September 2007)

In order to study the mechanism and parameters of hydrogen diffusion in the hexagonal (C14-type) Laves-phase ZrMn_2 , we have performed quasielastic neutron scattering measurements for ZrMn_2H_3 over the temperature range 10–390 K. It is found that the diffusive motion of hydrogen in this system can be described in terms of at least two jump processes: a fast localized H motion with the jump rate τ_l^{-1} and a slower process with the rate τ_d^{-1} associated with H jumps leading to long-range diffusion. The temperature dependence of τ_d^{-1} in the range 225–390 K follows the Arrhenius law with the activation energy of 124 ± 4 meV. In the same range, the temperature dependence of τ_l^{-1} deviates from the Arrhenius behavior and is considerably weaker than that of τ_d^{-1} . The Q dependence of the elastic incoherent structure factor (studied up to $Q_{\max} \approx 3.8 \text{ \AA}^{-1}$) suggests that the fast localized H motion in ZrMn_2H_3 corresponds to two-site jumps within pairs of closely spaced interstitial Zr_2Mn_2 sites.

DOI: 10.1103/PhysRevB.76.104305

PACS number(s): 66.30.Jt, 78.70.Nx

I. INTRODUCTION

Hydrogen diffusion in Laves-phase intermetallic compounds AB_2 shows a number of interesting features including high H mobility down to low temperatures, unusual isotope effects, and a coexistence of two frequency scales of H jump motion.¹ For the cubic (C15-type) Laves phases, the microscopic picture of H jumps and the systematics of the two frequency scales of H motion are well understood.^{1–5} In most of the studied cubic Laves phases where H atoms occupy only tetrahedral interstitial sites of g type (A_2B_2), the faster jump process corresponds to the localized H motion within the hexagons formed by g sites, and the slower process (leading to long-range diffusion) is associated with H jumps from one g -site hexagon to another. The difference between the characteristic frequencies of these jump processes is believed to result from the difference between the g - g distances r_1 (within the hexagon) and r_2 (between the nearest hexagons).

In contrast to the cubic Laves phases, the information on hydrogen diffusion in the hexagonal (C14-type) Laves phases is still fragmentary. The mobility of hydrogen has been studied in C14-type $\text{Ti}_{1.2}\text{Mn}_{1.8}\text{H}_3$,⁶ ZrMn_2H_x ,⁷ $\text{TiCr}_{1.9}\text{H}_x$,⁸ ZrCr_2H_x ,^{9–12} and HfCr_2H_x .¹³ In all these systems, H mobility is found to be very high. For example, the measured hydrogen diffusion coefficient in $\text{ZrCr}_2\text{H}_{0.5}$ is about $5 \times 10^{-7} \text{ cm}^2/\text{s}$ at 300 K.¹² However, the atomic-scale mechanism of H jump motion in C14-type compounds has not been elucidated thus far. Both the frequency and spatial scales of H jump motion can be probed by quasielastic neutron scattering (QENS) measurements.^{14,15} While previous results of QENS experiments on C14-type $\text{Ti}_{1.2}\text{Mn}_{1.8}\text{H}_3$,⁶ $\text{ZrCr}_2\text{H}_{0.5}$,¹² and $\text{HfCr}_2\text{H}_{0.74}$ (Ref. 13) suggest a coexistence of at least two H jump processes with different characteristic rates, no definitive conclusions about the nature of the faster jump process in these systems have been made. This can be related to the following factors. (1) The sublattice of interstitial A_2B_2 sites in C14-type Laves phases is more complex than that in C15-type Laves phases. Therefore, more com-

plex models may be required for analysis of the QENS data. (2) The range of the neutron momentum transfers in Refs. 6, 12, and 13 was insufficient to distinguish unambiguously between different models of localized H motion. The aim of the present work is to study the microscopic picture and the parameters of H jump motion in C14-type ZrMn_2H_x using QENS measurements over a wider range of the neutron momentum transfer.

The intermetallic compound ZrMn_2 is known to have some unusual physical properties.¹⁶ It can also absorb large amounts of hydrogen [up to 3.6 H atoms per formula unit (Ref. 17)]. According to neutron diffraction measurements,¹⁸ at room temperature, the deuteride ZrMn_2D_3 retains the hexagonal C14-type host-metal lattice (space group $P6_3/mmc$), and D atoms randomly occupy four types of tetrahedral interstitial sites formed by two Zr and two Mn atoms. Below $T \approx 230$ K, the neutron diffraction experiments¹⁹ have revealed an ordering of D atoms in ZrMn_2D_3 . The ordered distribution of D atoms in the low-temperature phase has not been elucidated;¹⁹ however, the metal atoms are found to retain the undistorted C14-type structure. The neutron diffraction measurements¹⁹ are also consistent with a second-order magnetic phase transition in ZrMn_2D_3 at $T \approx 175$ K. In the present work, we report the QENS results for ZrMn_2H_3 over the temperature range 225–390 K. These results are compared with those for other Laves-phase hydrides.

II. EXPERIMENTAL DETAILS

The ZrMn_2 compound was prepared by arc melting high-purity Zr and Mn in a helium atmosphere. The resulting single-phase intermetallic was found to have the hexagonal C14-type structure with the lattice parameters $a = 5.037 \text{ \AA}$ and $c = 8.275 \text{ \AA}$. Small pieces of ZrMn_2 were hydrogenated in a Sieverts-type vacuum system. After annealing the sample in vacuum at $650 \text{ }^\circ\text{C}$ for 1 h, H_2 gas at the pressure of 1.8 bar was admitted to the system, and the sample was then slowly cooled down to room temperature in a hydrogen

atmosphere. The amount of absorbed hydrogen (3.0 ± 0.1 H atoms per formula unit) was determined from the pressure drop in the calibrated volume of the system. According to x-ray diffraction analysis, the ZrMn_2H_3 sample is a single-phase compound with the C14-type host lattice and the lattice parameters $a=5.418 \text{ \AA}$ and $c=8.817 \text{ \AA}$. These values of the lattice parameters are close to those reported earlier for ZrMn_2D_3 .^{18,19}

QENS measurements were performed on the Fermi-chopper time-of-flight spectrometer (FCS) and on the disk-chopper time-of-flight spectrometer (DCS) at the NIST Center for Neutron Research. The temperature dependence of QENS spectra $S_{\text{exp}}(Q, \omega)$ (where $\hbar\omega$ is the energy transfer and $\hbar Q$ is the elastic momentum transfer) was measured in the range 225–390 K using FCS with the incident neutron wavelength $\lambda=4.8 \text{ \AA}$. For this configuration, the energy resolution was $145 \mu\text{eV}$ (full width at half-maximum), and the Q range studied was $0.58\text{--}2.42 \text{ \AA}^{-1}$. At two temperatures ($T=250$ and 360 K), QENS spectra were also measured using FCS with $\lambda=4.08 \text{ \AA}$ and DCS with $\lambda=3.0 \text{ \AA}$. These measurements allowed us to extend the Q range probed to higher values. The energy resolution and the Q range were $255 \mu\text{eV}$ and $0.68\text{--}2.85 \text{ \AA}^{-1}$, respectively for FCS and $200 \mu\text{eV}$ and $0.61\text{--}3.78 \text{ \AA}^{-1}$ for DCS. The powdered ZrMn_2H_3 sample was measured in a hollow-cylinder Al container, the sample thickness being 0.3 mm . The sample thickness was chosen to ensure $\sim 90\%$ neutron transmission and thus minimize multiple scattering effects. For data analysis, the detectors were binned into nine groups. The scattering angles corresponding to the Bragg reflections were excluded from the analysis. The instrumental resolution functions were determined from the measured QENS spectra of ZrMn_2H_3 at low temperatures (37 K for FCS with $\lambda=4.8 \text{ \AA}$, 40 K for FCS with $\lambda=4.08 \text{ \AA}$, and 10 K for DCS with $\lambda=3.0 \text{ \AA}$).

III. RESULTS AND DISCUSSION

A. Quasielastic neutron scattering spectra

QENS spectra for ZrMn_2H_3 measured at $T=225$ and 250 K can be reasonably described by a sum of two components: an “elastic” line represented by the spectrometer resolution function $R(Q, \omega)$ and a resolution-broadened Lorentzian “quasielastic” line. The relative intensity of the quasielastic component is found to increase with increasing Q , its half-width being nearly Q independent. However, at higher temperatures ($T > 250 \text{ K}$), the description in terms of a sum of an elastic line and a single Lorentzian quasielastic component leads to systematic deviations of the model QENS spectra from the experimental ones. For these temperatures, we have to add a second Lorentzian quasielastic component, so that the experimental scattering function $S_{\text{exp}}(Q, \omega)$ is fitted with the incoherent scattering function,

$$S_{\text{inc}}(Q, \omega) = A_0(Q)\delta(\omega) + A_1(Q)L(\omega, \Gamma_1) + A_2(Q)L(\omega, \Gamma_2), \quad (1)$$

convoluted with $R(Q, \omega)$. Here, $\delta(\omega)$ is the elastic δ function, $L(\omega, \Gamma_i)$ are the Lorentzian functions with the half-widths Γ_i , and $A_0 + A_1 + A_2 = 1$. As an example of the data, Fig. 1 shows

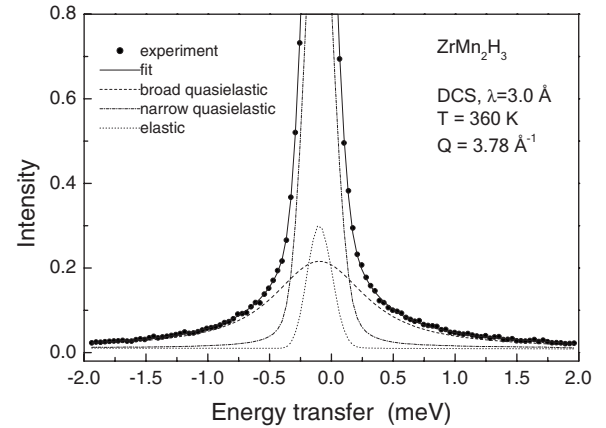


FIG. 1. The QENS spectrum for ZrMn_2H_3 measured on DCS at $T=360 \text{ K}$ and $Q=3.78 \text{ \AA}^{-1}$. The circles are the experimental points interpolated to the uniform energy grid. The full curve shows the fit of the three-component model [Eq. (1)] to the data. The dotted line represents the elastic component (the spectrometer resolution function), and the broken curves show two Lorentzian quasielastic components.

the QENS spectrum of ZrMn_2H_3 measured on DCS ($\lambda=3.0 \text{ \AA}$) at $T=360 \text{ K}$ and $Q=3.78 \text{ \AA}^{-1}$. At the first stage of the analysis, we have used the model scattering function [Eq. (1)] with two amplitudes ($A_0, A_1, A_2=1-A_0-A_1$) and two half-widths (Γ_1, Γ_2) being independent fit parameters. This model also improves the description of the QENS spectra measured at $T=225$ and 250 K . At all the temperatures studied, the intensity of the broader quasielastic component, $A_2(Q)$, is found to increase with increasing Q , and its half-width Γ_2 appears to be nearly Q independent. Since these features are typical of a spatially confined atomic motion,^{14,15} the broad quasielastic component is attributed to a fast localized H motion with the jump rate τ_1^{-1} . In this case, the value of Γ_2 should be proportional to τ_1^{-1} , while the Q dependence of A_2 should be related to the geometry of this motion.

The half-width of the narrow quasielastic component, Γ_1 , is found to increase with increasing Q and to pass through a broad maximum in the Q range $2.4\text{--}3.0 \text{ \AA}^{-1}$. Furthermore, the values of Γ_1 rapidly increase with increasing temperature. These features suggest that the narrow quasielastic component originates from a jump process leading to long-range H diffusion. The intensity of the elastic component, A_0 , is found to be small (about 9% of the total scattered intensity) and nearly Q and T independent. This component can be attributed to the residual elastic contribution due to the scattering on host-metal nuclei and, possibly, on some trapped protons.

Since A_0 and Γ_2 appear to be nearly Q independent, at the next stage of the analysis, these parameters have been fixed (being equal to their average values at a given temperature). Thus, only A_1 and Γ_1 remain to be independent fit parameters. In this case, the fitting procedure becomes quite stable. The solid curve in Fig. 1 shows the fit of the three-component model [Eq. (1)] to the data, and the broken curves represent contributions of the different components.

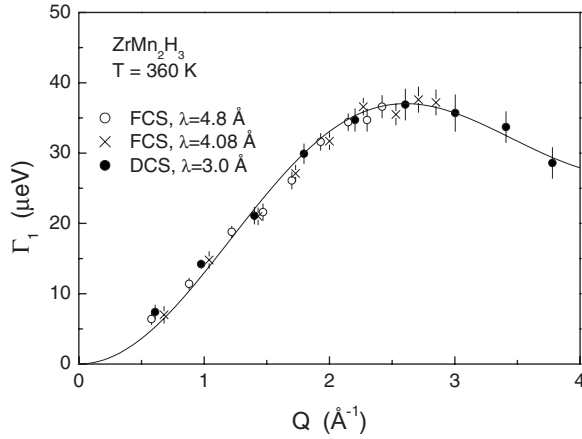


FIG. 2. The half-width at half-maximum (HWHM) of the narrow Lorentzian QENS component for ZrMn_2H_3 as a function of Q measured at $T=360$ K using FCS with $\lambda=4.8$ and 4.08 Å and DCS with $\lambda=3.0$ Å. The full curve shows the fit of the Chudley-Elliott model [Eq. (2)] to the data.

B. Parameters of hydrogen motion: Long-range diffusion

The Q dependences of the half-width Γ_1 of the narrow quasielastic line, as derived from the QENS spectra measured at several temperatures, are shown in Figs. 2 and 3. For the measurements at other temperatures, the $\Gamma_1(Q)$ dependences have similar shapes. As can be seen from Fig. 2, there is a satisfactory agreement between the results obtained using different spectrometers at different values of the incident neutron wavelength. Figure 2 also demonstrates the importance of the Q -range extension: the $\Gamma_1(Q)$ maximum manifests itself only in the data set corresponding to $\lambda=3.0$ Å. For parametrization of the $\Gamma_1(Q)$ dependence, we have used the orientationally averaged Chudley-Elliott model.²⁰ The corresponding form of $\Gamma_1(Q)$ is

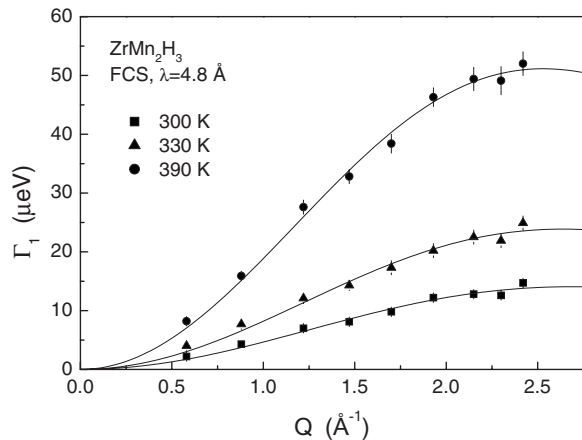


FIG. 3. The HWHM of the narrow Lorentzian QENS component for ZrMn_2H_3 as a function of Q measured at $T=300$, 330 , and 390 K using FCS with $\lambda=4.8$ Å. The full curves show the fits of the Chudley-Elliott model [Eq. (2)] to the data.

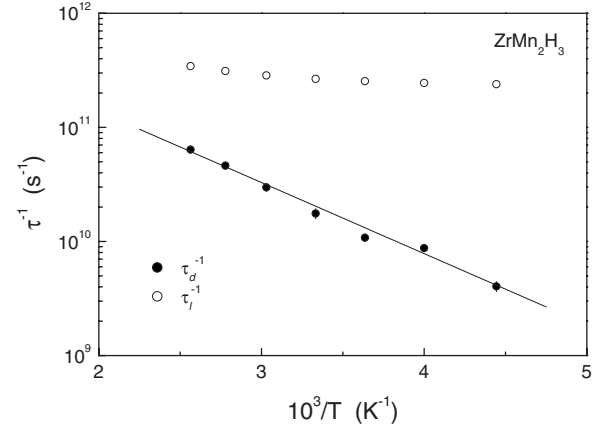


FIG. 4. The hydrogen jump rates τ_d^{-1} and τ_l^{-1} in ZrMn_2H_3 as functions of the inverse temperature. The full line shows the Arrhenius fit to the data for τ_d^{-1} .

$$\Gamma_1(Q) = \frac{\hbar}{\tau_d} \left(1 - \frac{\sin QL}{QL} \right), \quad (2)$$

where τ_d is the mean time between two successive H jumps leading to long-range diffusion, and L is the effective jump length. The fits of Eq. (2) to the data are shown by the solid curves in Figs. 2 and 3. The temperature dependence of the H jump rate τ_d^{-1} resulting from the Chudley-Elliott fits is presented in Fig. 4. This temperature dependence can be satisfactorily described by the Arrhenius law

$$\tau_d^{-1} = \tau_{d0}^{-1} \exp(-E_a^d/k_B T), \quad (3)$$

where E_a^d is the activation energy for hydrogen diffusion. The solid line in Fig. 4 shows the Arrhenius fit to the τ_d^{-1} data; the corresponding fit parameters are $\tau_{d0}^{-1} = (2.4 \pm 0.3) \times 10^{12} \text{ s}^{-1}$ and $E_a^d = 124 \pm 4 \text{ meV}$. This value of E_a^d should be compared to that estimated previously from the proton spin-spin relaxation measurements for ZrMn_2H_3 , $E_a^d = 150 \pm 9 \text{ meV}$.⁷ Note that the activation energy for long-range H diffusion in ZrMn_2H_3 is one of the lowest among Laves-phase hydrides.¹ Because of the low E_a^d , the hydrogen diffusion in ZrMn_2H_3 is observable by time-of-flight QENS even below room temperature.

The values of L derived from the Chudley-Elliott fits are close to 1.7 Å, tending to increase slightly with increasing temperature. It should be noted that the fitted values of the effective jump length are longer than the distances between the nearest-neighbor Zr_2Mn_2 interstitial sites (~ 1.2 Å) in ZrMn_2H_3 . This feature appears to be common for a number of Laves-phase hydrides.^{1,2,4,12,21,22} It will be discussed in more detail in Sec. III C.

The relation between the tracer diffusion coefficient D and the values of τ_d and L is given by

$$D = \frac{L^2}{6\tau_d}. \quad (4)$$

We assume here that the tracer correlation factor²³ for H diffusion is equal to 1. This assumption is only valid at low H concentrations. In ZrMn_2H_3 , one-fourth of all available

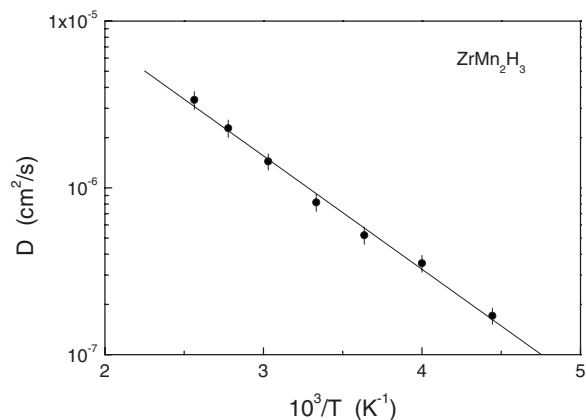


FIG. 5. The temperature dependence of the tracer diffusion coefficient of hydrogen in ZrMn_2H_3 derived from the Chudley-Elliott fits [Eqs. (2) and (4)]. The full line shows the Arrhenius fit to the data.

Zr_2Mn_2 interstitial sites are occupied by H atoms. For this occupancy, the absolute values of D determined from Eq. (4) may be overestimated by up to 20%. However, the relative changes in D with temperature should be described correctly. Figure 5 shows the temperature dependence of the tracer diffusion coefficient derived from Eq. (4) using the values of τ_d and L obtained from the Chudley-Elliott fits. The solid line in Fig. 5 represents the Arrhenius fit to the $D(T)$ data; the corresponding fit parameters are the activation energy $E_a^D = 135 \pm 5$ meV and the pre-exponential factor $D_0 = (1.7 \pm 0.3) \times 10^{-4}$ cm²/s. The resulting activation energy for D appears to be somewhat higher than that for τ_d^{-1} ; this is related to the previously mentioned slow increase in L with increasing temperature. The value of D_0 for ZrMn_2H_3 is of the same order of magnitude as the corresponding values for other Laves-phase hydrides.¹

C. Localized hydrogen motion

The geometry of the localized H motion can, in principle, be derived from the Q dependence of the elastic incoherent structure factor (EISF).^{14,15} For QENS spectra described by Eq. (1), the “resolution-limited” EISF is defined as $(A_0 + A_1)/(A_0 + A_1 + A_2) = A_0 + A_1$. Assuming that the purely elastic component of these QENS spectra is dominated by the host-metal contribution to the incoherent scattering function, we can conclude that the EISF for the hydrogen sublattice is given by the ratio $A_1/(A_1 + A_2)$. As examples of the data, Figs. 6 and 7 show the Q dependences of the EISF for the H sublattice at several temperatures. For the measurements at other temperatures, the Q dependences of the EISF have similar shapes. As can be seen from Fig. 6, there is a reasonable agreement between the results obtained using different spectrometers at different values of the incident neutron wavelength. It is also evident that the measured EISF is temperature dependent, decreasing with increasing T . This feature is common for all the studied Laves-phase hydrides.^{1-5,12,13} In order to account for this feature, we have to assume that only a fraction p of the H atoms participates

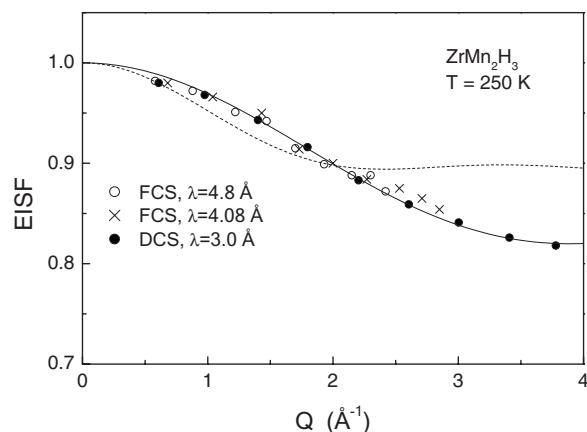


FIG. 6. The elastic incoherent structure factor for ZrMn_2H_3 as a function of Q measured at $T = 250$ K using FCS with $\lambda = 4.8$ and 4.08 Å and DCS with $\lambda = 3.0$ Å. The full curve shows the fit of the two-site model [Eq. (6)] to the data. The dashed curve shows the behavior of the EISF predicted by the six-site model [Eq. (5)] with the fixed $r = 1.22$ Å.

in the fast localized motion, and this fraction increases with temperature. The existence of a fraction $1 - p$ of “static” protons (on the frequency scale determined by the spectrometer resolution) is expected to originate from the H-H interaction leading to the formation of some ordered atomic configurations at low temperatures.² As the temperature increases, such ordered configurations should be progressively destroyed by thermal fluctuations; this results in the observed growth of p with increasing T .

We now turn to a discussion of the atomic-scale picture of the fast localized hydrogen motion in ZrMn_2H_3 . According to the neutron diffraction data for ZrMn_2D_3 ,¹⁸ hydrogen atoms occupy only the tetrahedral sites with Zr_2Mn_2 coordination. There are four inequivalent types of such sites in the C14-type lattice: $6h_1$, $6h_2$, $12k$, and $24l$. The spatial arrangement of these sites is shown in Fig. 8. As in the case of the C15-type structure, the sublattice of Zr_2Mn_2 sites consists of

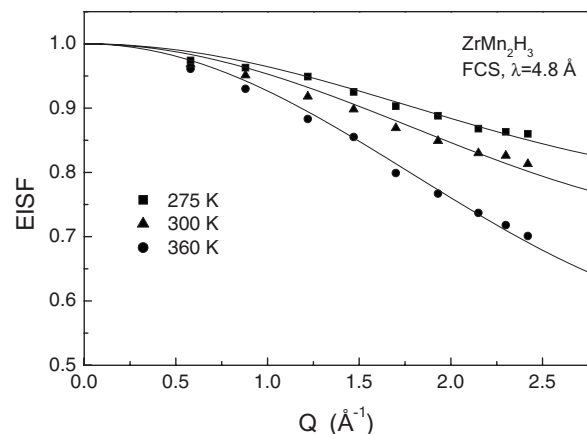


FIG. 7. The elastic incoherent structure factor for ZrMn_2H_3 as a function of Q measured at $T = 275$, 300, and 360 K using FCS with $\lambda = 4.8$ Å. The full curves show the fits of the two-site model [Eq. (6)] with the fixed $r_4 = 1.16$ Å to the data.

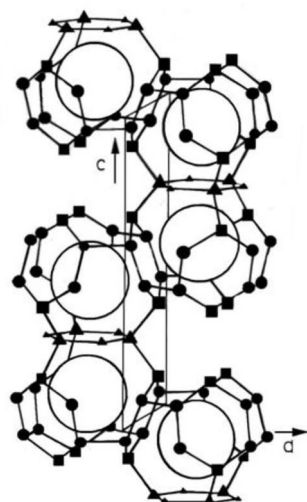


FIG. 8. The spatial arrangement of interstitial Zr_2Mn_2 sites in C14-type ZrMn_2 (from Ref. 18). Large triangles, h_1 sites; small triangles, h_2 sites; squares, k sites; solid circles, l sites; large open circles, Zr atoms.

hexagons; however, these hexagons are formed by inequivalent sites. Type I hexagons are in the basal plane; they are formed by alternating h_1 and h_2 sites. Type II hexagons are formed by two k and four l sites in the sequence $k-l-l-k-l-l$. The sublattice of interstitial Zr_2Mn_2 sites shown in Fig. 8 is characterized by five distances between the nearest neighbors: r_3 (h_1 - h_2 , within type I hexagons), r_4 (l - l , within type II hexagons), r_5 (k - l , within type II hexagons), r_6 (h_1 - k , between type I and type II hexagons), and r_7 (l - l , between two type II hexagons). The values of these distances obtained using the positional parameters of D atoms at h_1 , h_2 , k , and l sites in ZrMn_2D_3 (Ref. 18) are listed in Table I.

The structure of the sublattice of Zr_2Mn_2 sites suggests two possible models of localized H motion. The first possibility is that a hydrogen atom jumps over sites forming a hexagon. This model is consistent with the fact that the distances between the nearest sites within the hexagons (r_3, r_4, r_5) are somewhat shorter than the distances between the nearest sites on different hexagons (r_6, r_7), see Table I. Neglecting the difference between type I and type II hexagons, we may try to use the standard model of jumps between six equidistant sites on a circle of radius r (Refs. 14 and 15); the corresponding orientationally averaged form of the EISF is given by

$$\text{EISF} = 1 - p + \frac{p}{6} [1 + 2j_0(Qr) + 2j_0(Qr\sqrt{3}) + j_0(2Qr)], \quad (5)$$

where $j_0(x)$ is the spherical Bessel function of zeroth order and r is the weighted average of r_3 , r_4 , and r_5 . Such a model was used previously for the analysis of QENS data for C14-type ZrCr_2H_x (Ref. 12) and HfCr_2H_x .¹³

Since the shortest distance between Zr_2Mn_2 sites in ZrMn_2H_3 is r_4 (see Table I), the second possibility corresponds to back-and-forth H jumps between two l sites on type II hexagons. For the two-site model of the localized motion, the orientationally averaged EISF is given by

$$\text{EISF} = 1 - p + \frac{p}{2} [1 + j_0(Qr_4)]. \quad (6)$$

It should be noted that the period of the oscillatory Q dependence of the EISF described by Eqs. (5) and (6) is determined by the corresponding intersite distances (r or r_4), while the value of p is responsible only for the amplitude of these oscillations.

Comparison of the experimental Q dependences of the EISF with the models represented by Eqs. (5) and (6) indicates that only the two-site model is consistent with the data. The solid curve in Fig. 6 shows the fit of the two-site model [Eq. (6)] to the EISF data at $T=250$ K; the corresponding fit parameters are $p=0.296\pm 0.015$ and $r_4=1.15\pm 0.02$ Å. Note that the value of r_4 resulting from the fit is very close to the actual nearest-neighbor l - l distance (1.16 Å, see Table I). The two-site model with the fixed $r_4=1.16$ Å also gives a reasonable description of the EISF data at the other temperatures (see, for example, the solid curves in Fig. 7). The dashed curve in Fig. 6 shows the behavior predicted by the six-site model [Eq. (5)] with the fixed $r=1.22$ Å. It can be seen that, in the Q range 2.3–3.3 Å⁻¹, the six-site model predicts an increase of the EISF with increasing Q , whereas the experimental EISF *decreases* in this range. Thus, the six-site model is inconsistent with the observed Q dependence of the EISF.

For the two-site model, the relation between the half-width Γ_2 of the broader quasielastic line and the jump rate τ_l^{-1} of the localized H motion is given by¹⁴ $\Gamma_2=2\hbar\tau_l^{-1}$. The values of τ_l^{-1} derived from the half-widths of the broader quasielastic line at different temperatures are shown in Fig. 4. As can be seen from this figure, the temperature dependence of τ_l^{-1} is considerably weaker than that of τ_d^{-1} . This

TABLE I. The distances (in Å) between the nearest-neighbor A_2B_2 interstitial sites in C14-type hydrides.

Description	Notation	ZrMn_2D_3	$\text{ZrCr}_2\text{D}_{3.8}$	$\text{HfCr}_2\text{D}_{0.8}$
h_1 - h_2 (within type I hexagons)	r_3	1.22	1.25	1.04
l - l (within type II hexagons)	r_4	1.16	1.20	1.18
k - l (within type II hexagons)	r_5	1.25	1.19	1.12
h_1 - k (between type I and type II hexagons)	r_6	1.29	1.30	1.25
l - l (between two type II hexagons)	r_7	1.31	1.35	1.24

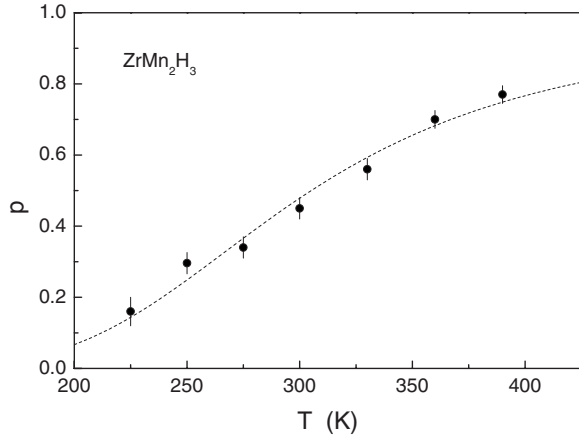


FIG. 9. The temperature dependence of the fraction of H atoms participating in the fast localized motion, as determined from the fits of the two-site model [Eq. (6)] to the data for ZrMn_2H_3 . The dashed line shows the fit of the model described by Eqs. (7) and (8) to $p(T)$.

feature is common for all the studied Laves-phase hydrides showing two frequency scales of H motion^{1,24} and is consistent with low barriers for the localized H motion. Furthermore, the temperature dependence of τ_l^{-1} seems to deviate from the Arrhenius behavior. It should be noted that the intensity of the broader quasielastic line decreases with decreasing temperature; this limits the τ_l^{-1} measurements at $T < 225$ K. Another limiting factor is the low-temperature ordering of hydrogen; according to the neutron diffraction measurements for ZrMn_2D_3 ,¹⁹ the ordering of D atoms occurs below 230 K. At room temperature, the jump rate τ_l^{-1} is a factor of 15 higher than τ_d^{-1} . The ratio τ_d/τ_l increases with decreasing temperature (up to 60 at 225 K).

The temperature dependence of p resulting from the fits of the two-site model to the EISF data is shown in Fig. 9. The usual approach to the description of $p(T)$ is based on the assumption of a certain energy gap ΔE between static and mobile H states (see, e.g., Ref. 25). In this case,

$$p(T) = \frac{b(T)}{1 + b(T)}, \quad (7)$$

$$b(T) = b_m \exp(-\Delta E/k_B T), \quad (8)$$

where b_m is the relative degeneracy factor of mobile states. The dashed line in Fig. 9 shows the fit of this model to $p(T)$; the resulting values of the fit parameters are $\Delta E = 132 \pm 9$ meV and $b_m = 150 \pm 50$. It should be noted, however, that in the studied range 225–390 K, the temperature dependence of p can also be described by other functions including a linear function.²

We now return to a discussion of the effective jump lengths L derived from the Chudley-Elliott analysis of $\Gamma_1(Q)$. As mentioned above, these values appear to be larger than the distances between the nearest-neighbor interstitial sites (r_3-r_7). This feature can be naturally accounted for in terms of the model of H motion with two frequency scales: the rate τ_l^{-1} of jumps within a small group of sites (in our case, within

a pair of l sites) and the rate τ_d^{-1} of jumps between such groups, $\tau_d^{-1} \ll \tau_l^{-1}$. As explained in Refs. 2 and 12, this model implies that τ_d is the mean residence time of a hydrogen atom at a group of closely spaced sites (not at a single interstitial site, as is commonly assumed). Since a hydrogen atom may enter an l - l pair through one site and leave it via another site, the total displacement for the time τ_d is the distance between the nearest sites at different l - l pairs plus the additional displacement between the initial and final positions of a hydrogen atom at the pair. The half-width Γ_1 is determined by the slower frequency scale τ_d^{-1} ; therefore, the apparent jump length L derived from the Q dependence of Γ_1 would be larger than the distances between the nearest-neighbor interstitial sites. More precisely, we expect a distribution of L values ranging from 1.31 Å (the nearest distance between l sites on different hexagons) to ~ 2.0 Å (the distance between the centers of two l - l pairs). Hence, the average value $L \approx 1.7$ Å derived from the Chudley-Elliott analysis seems to be reasonable.

Summarizing the results related to the microscopic picture of H motion in ZrMn_2H_3 , we conclude that the fastest H jump process corresponds to back-and-forth jumps within l - l pairs on type II hexagons. This localized motion determines the behavior of the broadest component of the QENS spectra. While the detailed microscopic picture of H motion may include even more than two frequency scales, our simplified description implies that all the slower jump processes are characterized by a single rate τ_d^{-1} responsible for the long-range H diffusion. In the temperature range 225–390 K, this rate is a factor of 5–60 lower than the jump rate τ_l^{-1} for the localized H motion.

D. Comparison with other Laves-phase hydrides

In order to discuss the systematics of H jump motion in hexagonal Laves phases, it is useful to compare the hydrogen sublattices in different C14-type hydrides. Included in Table I are the distances between the nearest-neighbor A_2B_2 sites partially occupied by hydrogen in C14-type $\text{ZrCr}_2\text{D}_{3,8}$ and $\text{HfCr}_2\text{D}_{0,8}$. These distances are derived from the room-temperature neutron diffraction measurements for $\text{ZrCr}_2\text{D}_{3,8}$ (Ref. 26) and $\text{HfCr}_2\text{D}_{0,8}$.²⁷ As can be seen from Table I, the relation between the distances r_3-r_7 changes from one compound to another. This results mainly from the fact that the positional parameters of hydrogen atoms at the same sites in different compounds differ from each other. The common feature of the hydrogen sublattices for all three compounds in Table I is that the distances r_6 and r_7 (between the sites on different hexagons) are longer than r_3 , r_4 , and r_5 (between the sites within type I and type II hexagons). However, the relations between r_3 , r_4 , and r_5 show significant changes from one compound to another. While for ZrMn_2D_3 the distance r_4 is definitely the shortest one, for $\text{ZrCr}_2\text{D}_{3,8}$, the shortest distances r_4 and r_5 are nearly the same. Therefore, the fastest H jump motion in ZrCr_2H_x is likely to be represented by H jumps within type II hexagons. For $\text{HfCr}_2\text{D}_{0,8}$, the shortest distance is r_3 , so that the fastest H jump motion in HfCr_2H_x can be attributed to localized H jumps within type I hexagons. It should be noted that the six-site localized

TABLE II. The parameters of hydrogen motion at 300 K for cubic and hexagonal Laves-phase hydrides. See text for details and sources of the data.

Parameter	$\text{TaV}_2\text{H}_{1.1}$	$\text{YMn}_2\text{H}_{0.6}$	$\text{ZrCr}_2\text{H}_{0.5}$	$\text{HfCr}_2\text{H}_{0.74}$	ZrMn_2H_3
Structural type	C15	C15	C14	C14	C14
R_A/R_B	1.090	1.425	1.250	1.232	1.267
Localized motion	Six-site	Two-site	Six-site	Six-site	Two-site
$\tau_l^{-1}(300\text{ K}) (\text{s}^{-1})$	3.8×10^{11}	6.4×10^{11}		5.6×10^{10}	2.7×10^{11}
$\tau_d^{-1}(300\text{ K}) (\text{s}^{-1})$	7.3×10^7	7.7×10^9	4.8×10^9	3.4×10^9	1.8×10^{10}
$\tau_d/\tau_l(300\text{ K})$	5.2×10^3	83		16	15
$D(300\text{ K}) (\text{cm}^2/\text{s})$	2.2×10^{-8}	8.9×10^{-7}	5.2×10^{-7}	3.4×10^{-7}	8.2×10^{-7}
$E_a^d (\text{meV})$	220	213	93	148	124

H motion is consistent with the QENS data for ZrCr_2H_x (Ref. 12) and HfCr_2H_x (Ref. 13) however, in Refs. 12 and 13, the actual positional parameters of hydrogen atoms were not taken into account, and the data were interpreted in terms of “average” hexagons.

The considerations presented above show that in hexagonal Laves-phase hydrides, the microscopic picture of H jump motion may change qualitatively from one compound to another. This situation is similar to that for cubic (C15-type) Laves-phase hydrides for which the fast localized H motion changes from six-site jumps in TaV_2H_x (Ref. 2) and HfMo_2H_x (Ref. 3) to two-site jumps in YMn_2H_x .⁵ For C15-type hydrides, such a change is related to the change in the structure of the sublattice of the A_2B_2 interstitial sites corresponding to the transition from $r_2 > r_1$ to $r_2 < r_1$. In turn, the ratio r_2/r_1 is determined mainly by the ratio of the metallic radii of the elements A and B , R_A/R_B ,^{1,24} being nearly independent of H concentration. It is likely that the ratio R_A/R_B also plays an important role for the mechanism of H motion in C14-type hydrides; however, the corresponding relation is difficult to define because of the complexity of the hydrogen sublattice in hexagonal Laves-phase hydrides.

In Table II, the motional parameters of hydrogen in ZrMn_2H_3 are compared with those in some other Laves-phase hydrides. Included in Table II are the data for two representative C15-type systems (TaV_2H_x and YMn_2H_x), as well as the data for all C14-type AB_2H_x systems studied by QENS. All the motional parameters of hydrogen in ZrMn_2H_3 result from the present work. The values of $\tau_l^{-1}(300\text{ K})$ are obtained from the time-of-flight QENS data for $\text{TaV}_2\text{H}_{1.1}$,² $\text{YMn}_2\text{H}_{0.6}$,⁵ and $\text{HfCr}_2\text{H}_{0.74}$.¹³ For C14-type ZrCr_2H_x , such data are not available. The values of $\tau_d^{-1}(300\text{ K})$ are estimated from the nuclear spin-lattice relaxation (NSLR) data for $\text{TaV}_2\text{H}_{1.15}$,²⁸ the time-of-flight QENS data for $\text{YMn}_2\text{H}_{0.65}$,²⁹ and the backscattering QENS data for $\text{ZrCr}_2\text{H}_{0.5}$ (Ref. 12) and $\text{HfCr}_2\text{H}_{0.74}$.¹³ The values of H diffusivity at 300 K are obtained from the backscattering QENS results for $\text{TaV}_2\text{H}_{1.1}$,² $\text{ZrCr}_2\text{H}_{0.5}$,¹² and $\text{HfCr}_2\text{H}_{0.74}$,¹³ and from the time-of-flight QENS results for $\text{YMn}_2\text{H}_{0.65}$.²⁹ The activation energies E_a^d for the slower jump rate τ_d^{-1} are derived from the NSLR measurements for $\text{TaV}_2\text{H}_{1.15}$,²⁸ the combined time-of-flight and backscattering QENS measurements for $\text{YMn}_2\text{H}_{0.65}$ (Ref. 29) and $\text{HfCr}_2\text{H}_{0.74}$,¹³ and the backscattering QENS measurements for $\text{ZrCr}_2\text{H}_{0.5}$.¹²

As can be seen from Table II, the value of $\tau_d^{-1}(300\text{ K})$ for ZrMn_2H_3 is higher than for the other studied Laves-phase hydrides. The jump rate of the localized H motion at room temperature, $\tau_l^{-1}(300\text{ K})$, for ZrMn_2H_3 is somewhat lower than for C15-type $\text{TaV}_2\text{H}_{1.1}$ and $\text{YMn}_2\text{H}_{0.6}$. The ratio of the characteristic jump rates, $\tau_d/\tau_l(300\text{ K})$, for ZrMn_2H_3 is close to that for C14-type $\text{HfCr}_2\text{H}_{0.74}$, being considerably lower than for C15-type compounds. Note that the moderate values of τ_d/τ_l in C14-type hydrides allow one to probe both frequency scales of H motion at a certain temperature in a single experiment using a time-of-flight spectrometer. For compounds with high τ_d/τ_l ratios (such as C15-type TaV_2H_x), both frequency scales can be probed only by combining two experimental techniques, for example, time-of-flight QENS and backscattering QENS or NSLR measurements.

IV. CONCLUSIONS

The analysis of our quasielastic neutron scattering data for C14-type ZrMn_2H_3 has shown that the diffusive motion of hydrogen in this system can be described in terms of at least two jump processes with different characteristic frequencies. The faster process with the jump rate τ_l^{-1} corresponds to localized H motion, and the slower process with the jump rate τ_d^{-1} is associated with H jumps leading to long-range diffusion. The ratio of the jump rates for these two processes, τ_d/τ_l , is found to change from 5 at 390 K to 60 at 225 K. For the localized motion, our results are consistent with back-and-forth jumps of H atoms within pairs of closely spaced $24l$ sites. Comparison of the structural and QENS results for ZrMn_2H_3 with those for C14-type ZrCr_2H_x and HfCr_2H_x shows that small changes in the structure of the hydrogen sublattice may lead to a qualitative change in the mechanism of H motion.

The temperature dependence of the slower jump rate τ_d^{-1} for ZrMn_2H_3 in the range 225–390 K can be reasonably described by the Arrhenius law with the activation energy $E_a^d = 124 \pm 4$ meV and the pre-exponential factor $\tau_{d0}^{-1} = (2.4 \pm 0.3) \times 10^{12} \text{ s}^{-1}$. In the same range, the temperature dependence of τ_l^{-1} deviates from the Arrhenius behavior, being considerably weaker than that of τ_d^{-1} .

ACKNOWLEDGMENTS

The authors are grateful to C. M. Brown, V. I. Voronin, and O. A. Babanova for assistance with the data analysis. This work utilized facilities supported in part by the National Science Foundation under Agreement No. DMR-0454672.

This work was also supported by the Russian Foundation for Basic Research (Grant No. 06-02-16246) and the Priority Program “Basic energy problems” of the Russian Academy of Sciences. A.V.S. acknowledges financial support from the NIST Center for Neutron Research.

-
- ¹A. V. Skripov, *Defect Diffus. Forum* **224-225**, 75 (2003).
²A. V. Skripov, J. C. Cook, D. S. Sibirtsev, C. Karmonik, and R. Hempelmann, *J. Phys.: Condens. Matter* **10**, 1787 (1998).
³A. V. Skripov, J. C. Cook, T. J. Udovic, and V. N. Kozhanov, *Phys. Rev. B* **62**, 14099 (2000).
⁴D. J. Bull, D. P. Broom, and D. K. Ross, *Chem. Phys.* **292**, 153 (2003).
⁵A. V. Skripov, M. A. Gonzalez, and R. Hempelmann, *J. Phys.: Condens. Matter* **18**, 7249 (2006).
⁶R. Hempelmann, D. Richter, and A. Heidemann, *J. Less-Common Met.* **88**, 343 (1982).
⁷J. Shinar, D. Davidov, D. Shaltiel, and N. Kaplan, *Z. Phys. Chem., Neue Folge* **117**, 69 (1979).
⁸R. C. Bowman, B. D. Craft, A. Attalla, and J. R. Johnson, *Int. J. Hydrogen Energy* **8**, 801 (1983).
⁹K. Morimoto, M. Saga, H. Fujii, T. Okamoto, and T. Hihara, *J. Phys. Soc. Jpn.* **57**, 647 (1988).
¹⁰A. V. Skripov, M. Yu. Belyaev, and A. P. Stepanov, *Solid State Commun.* **78**, 909 (1991).
¹¹W. Renz, G. Majer, A. V. Skripov, and A. Seeger, *J. Phys.: Condens. Matter* **6**, 6367 (1994).
¹²A. V. Skripov, M. Pionke, O. Randl, and R. Hempelmann, *J. Phys.: Condens. Matter* **11**, 1489 (1999).
¹³A. V. Skripov, A. V. Soloninin, A. L. Buzlukov, L. S. Voyevodina, J. C. Cook, T. J. Udovic, and R. Hempelmann, *J. Phys.: Condens. Matter* **17**, 5011 (2005).
¹⁴M. Bée, *Quasielastic Neutron Scattering* (Hilger, Bristol, 1988).
¹⁵R. Hempelmann, *Quasielastic Neutron Scattering and Solid State Diffusion* (Clarendon, Oxford, 2000).
¹⁶M. Rotter, A. Grytsiv, X. Q. Chen, P. Rogl, R. Podloucky, W. Wolf, V. T. Witusiewicz, A. Saccone, H. Noel, M. Doerr, A. Lindbaum, H. Michor, E. Bauer, S. Heathman, W. Kockelmann, and J. Taylor, *Phys. Rev. B* **74**, 224109 (2006).
¹⁷D. Shaltiel, I. Jacob, and D. Davidov, *J. Less-Common Met.* **53**, 117 (1977).
¹⁸J. J. Didisheim, K. Yvon, D. Shaltiel, and P. Fischer, *Solid State Commun.* **31**, 47 (1979).
¹⁹J. J. Didisheim and P. Fischer, *J. Less-Common Met.* **103**, 267 (1984).
²⁰C. T. Chudley and R. J. Elliott, *Proc. Phys. Soc. London* **77**, 353 (1961).
²¹R. L. Havill, J. M. Titman, M. S. Wright, and M. A. Crouch, *Z. Phys. Chem., Neue Folge* **164**, 1083 (1989).
²²S. I. Campbell, M. Kemali, D. K. Ross, D. J. Bull, J. F. Fernandez, and M. R. Johnson, *J. Alloys Compd.* **293-295**, 351 (1999).
²³R. A. Tahir-Kheli and R. J. Elliott, *Phys. Rev. B* **27**, 844 (1983).
²⁴A. V. Skripov, *J. Alloys Compd.* **404-406**, 224 (2005).
²⁵N. F. Berk, J. J. Rush, T. J. Udovic, and I. S. Anderson, *J. Less-Common Met.* **172-174**, 496 (1991).
²⁶A. V. Irodova and E. Suard, *J. Alloys Compd.* **299**, 32 (2000).
²⁷A. V. Skripov, T. J. Udovic, and Q. Huang (unpublished).
²⁸A. V. Skripov, S. V. Rychkova, M. Yu. Belyaev, and A. P. Stepanov, *J. Phys.: Condens. Matter* **2**, 7195 (1990).
²⁹A. V. Skripov, J. C. Cook, T. J. Udovic, M. A. Gonzalez, R. Hempelmann, and V. N. Kozhanov, *J. Phys.: Condens. Matter* **15**, 3555 (2003).